



Phase-detected Brillouin optical correlation-domain reflectometry

Yosuke Mizuno¹ · Neisei Hayashi² · Hideyuki Fukuda³ · Kentaro Nakamura¹

Received: 21 November 2017 / Accepted: 3 April 2018 / Published online: 2 May 2018
© The Optical Society of Japan 2018

Abstract

Optical fiber sensing techniques based on Brillouin scattering have been extensively studied for structural health monitoring owing to their capability of distributed strain and temperature measurement. Although a higher signal-to-noise ratio (leading to high spatial resolution and high-speed measurement) is generally obtained for two-end-access systems, they reduce the degree of freedom in embedding the sensors into structures, and render the measurement no longer feasible when extremely high loss or breakage occurs at a point of the sensing fiber. To overcome these drawbacks, a one-end-access sensing technique called Brillouin optical correlation-domain reflectometry (BOCDR) has been developed. BOCDR has a high spatial resolution and cost efficiency, but its conventional configuration suffered from relatively low-speed operation. In this paper, we review the recently developed high-speed configurations of BOCDR, including phase-detected BOCDR, with which we demonstrate real-time distributed measurement by tracking a propagating mechanical wave. We also demonstrate breakage detection with a wide strain dynamic range.

Keywords Brillouin scattering · Distributed strain and temperature sensing · High-speed measurement · Nonlinear optics · Optical fiber sensors

1 Introduction

Fiber-optic Brillouin scattering [1] has been widely exploited to perform distributed measurement of strain and temperature. The Brillouin-based distributed sensors developed thus far can be classified into two categories. One is “analysis”, in which two light beams are injected into both ends of a fiber under test (FUT), and the other is “reflectometry”, in

which a single light beam is injected into one end of an FUT. The former includes Brillouin optical time-domain analysis (BOTDA) [2–12], Brillouin optical frequency-domain analysis (BOFDA) [13–16], and Brillouin optical correlation-domain analysis (BOCDA) [12, 17–24], while the latter includes Brillouin optical time-domain reflectometry (BOTDR) [25–29], Brillouin optical frequency-domain reflectometry (BOFDR) [30], and Brillouin optical correlation-domain reflectometry (BOCDR) [31–36]. A variety of configurations have been proposed for each technique to improve the performance, such as spatial resolution, measurement range, signal-to-noise ratio (SNR), sampling rate, repetition rate, strain and temperature sensitivity, strain (or temperature) dynamic range, system simplicity, and cost efficiency. Here, let us focus mainly on Brillouin sensors with a high sampling (or repetition) rate.

Extremely high sampling rates have already been achieved in BOTDA [3–11] and BOCDA [19, 20, 24]. Inspired by the idea of Bernini et al. [4], Peled et al. [5] have also developed a high-speed configuration of BOTDA called slope-assisted BOTDA, which interrogates the FUT with a single frequency located at the middle of the slope of the local Brillouin gain spectrum (BGS) and enables a single

✉ Yosuke Mizuno
ymizuno@sonic.pi.titech.ac.jp

Neisei Hayashi
hayashi@cntp.t.u-tokyo.ac.jp

Hideyuki Fukuda
fahrenheitniku@gmail.com

Kentaro Nakamura
knakamur@sonic.pi.titech.ac.jp

¹ Institute of Innovative Research, Tokyo Institute of Technology, Midori-ku, Yokohama 226-8503, Japan

² Research Center for Advanced Science and Technology, The University of Tokyo, Meguro-ku, Tokyo 153-8904, Japan

³ Servo Laboratory, FANUC Corporation, Oshino-mura, Yamanashi 401-0597, Japan

pump pulse to sample the strain distribution along the full length of the FUT. By synthesizing an adaptable probe wave, an FUT with an arbitrary Brillouin frequency shift (BFS) distribution can be interrogated, though the strain dynamic range is limited by the size of the linear section of the BGS. Peled et al. [6] have also demonstrated dynamic BOTDA measurements by implementing the fast switching of optical frequency using high-performance arbitrary-waveform generators, though the measurement time becomes longer with increasing FUT length. Furthermore, Taki et al. [7] have proposed using cyclic pulse coding based on quasi-periodic bit sequences in BOTDA for an FUT with a length on the order of kilometers. This configuration can substantially reduce the number of averages required to guarantee an acceptable SNR. Many other efforts to improve the performance of high-speed BOTDA have been made [3, 8–11]. High-speed operation has also been achieved by BOFDA. Song et al. [19] have obtained a 1 kHz sampling rate at a single location using a time-division pump–probe generation scheme with optimized temporal gates and an unbalanced Mach–Zehnder delay line. They have also demonstrated a distributed measurement over a 100 m long FUT at a 20 Hz repetition rate with 80 cm spatial resolution using differential frequency modulation [20]. In addition, random accessibility with a 5 kHz sampling rate has been demonstrated at the cost of the employment of a high-speed lock-in amplifier [24]. Thus, only analysis systems based on stimulated Brillouin scattering (SBS), not on spontaneous scattering, have been used to perform real-time Brillouin measurement with higher (sub-meter) spatial resolution.

In general, SBS is induced by a so-called pump–probe configuration, which has, however, two problems from a practical viewpoint. First, the pump and probe lights need to be injected into both ends of the FUT, which is not convenient for embedding the sensors into materials and structures; besides, the measurement turns out no longer feasible when breakage (or extremely high loss) occurs at a point along the FUT. Some quasi-one-end-access configurations [16, 21, 22] developed by exploiting the Fresnel reflection at the open end of an FUT cannot perfectly overcome the measurement difficulties associated with a breakage point. The other problem is that a relatively expensive electro-optic modulator (EOM), such as a single-sideband modulator, is often needed to accurately produce the frequency difference between the pump and probe lights [3–18, 20–24]. Moreover, most configurations require an additional EOM for optical pulse generation [2–12] or chopping for lock-in detection [17, 18, 20–24]. Although a time-division pump–probe generation scheme [19] does not require an EOM for pump/probe generation, the driving current of the laser diode (LD) needs to be precisely controlled. Furthermore, it is notable that some systems suffer from another problem—a limited strain dynamic range. For instance, the largest strain that

can be measured is, in principle, limited by the Brillouin bandwidth in slope-assisted BOTDA [4, 5] and by the non-negligible correlation peak sidelobes in BOFDA [23]. Thus, it is crucial to develop distributed Brillouin sensing technology that simultaneously provides a high sampling/repetition rate, intrinsically one-end-access interrogation, high spatial resolution, wide strain dynamic range, high SNR, and system simplicity (thereby leading to cost efficiency). Considering the first two requirements, it appears that BOTDR is not suitable because the spontaneous-Brillouin-scattered signal generated by incident optical pulses is so weak that the signal needs to be integrated a number of times [25–29], although there are some trials reported [37].

In this review paper, we describe recently developed high-speed configurations of BOCDR [38, 39], which potentially satisfy all the aforementioned advantages simultaneously. BOCDR is known to be an intrinsically one-end-access sensing technique with high spatial resolution, system simplicity, and cost efficiency. Here, the frequency sweeping for acquiring the BGS is performed at high speed without using the inherent sweeping function of an electrical spectrum analyzer (ESA), which is used only to detect the signal power at a fixed frequency component. The noise caused by the external frequency sweeping is suppressed by obtaining the differential signal between periods of operation with and without the Brillouin signal, resulting in a high SNR and enhanced strain dynamic range. The additionally required main devices only include a relatively low-performance frequency sweeper [or a standard voltage-controlled oscillator (VCO)] and an inexpensive sound board connected to a computer, thereby maintaining the system simplicity and cost efficiency. We also implement high-speed BFS acquisition from the BGS (“phase-detected BOCDR”) and show that the BFS (at one position) can be derived at > 100 kHz at the sacrifice of the limited range of measurable strain. A variety of measurement examples (including breakage detection and the tracking of a propagating mechanical wave) are presented, demonstrating the high performance of this high-speed BOCDR.

2 High-speed configuration

2.1 Principle and proposal

As mentioned above, BOCDR [31, 32] is a distributed sensing technique with intrinsic one-end accessibility and high spatial resolution. Its operating principle is based on the correlation control of continuous lightwaves in a self-heterodyne scheme. Specifically speaking, the pump light and the reference light (instead of the probe light used in BOFDA) are sinusoidally frequency-modulated at f_m , and periodical “correlation peaks [40]” are generated in

the FUT. The measurement range d_m is determined by the interval between the correlation peaks, which is inversely proportional to f_m as [32]:

$$d_m = \frac{c}{2nf_m}, \tag{1}$$

where c is the velocity of light in a vacuum and n is the refractive index of the fiber core. By sweeping f_m , the correlation peak, which can be regarded as the sensing position, is scanned along the fiber to acquire a BGS or BFS distribution. The spatial resolution Δz is given by [32]:

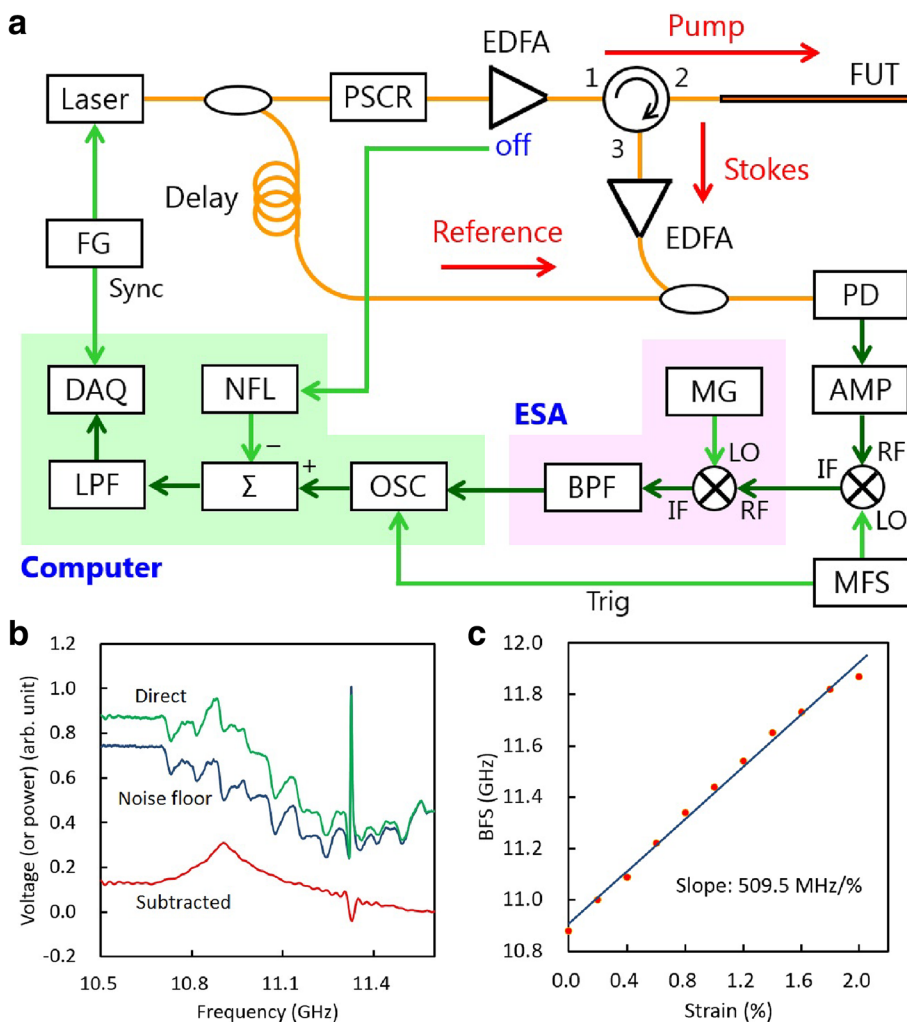
$$\Delta z = \frac{c \Delta\nu_B}{2\pi n f_m \Delta f}, \tag{2}$$

where $\Delta\nu_B$ is the Brillouin bandwidth [typically 30 MHz in silica single-mode fibers (SMFs)] and Δf is the modulation amplitude of the optical frequency. Note that Δf is practically limited to a half of the BFS of the FUT due to the Rayleigh noise [31, 32]. The highest sampling rate reported so far, including data acquisition to the computer, was 19 Hz

[33], and was limited by the frequency sweeping speed of an ESA. The maximal measurable strain experimentally confirmed was 0.3% (low SNR) in a temporal gating scheme [34], 0.32% (higher SNR) with noise floor compensation [35], and 0.7% (low SNR) in an intensity-modulation-based apodization scheme [36].

Figure 1a depicts the experimental setup of the high-speed configuration of BOCADR [38]. The fiber-optic parts are similar to those previously reported [35]. The 7 dBm output from a distributed-feedback LD with a line width of ~1 MHz was divided into two lights (pump and reference) using an optical coupler. The pump light was led to a polarization scrambler (PSCR) to suppress the polarization-dependent fluctuations of the BGS, amplified using an erbium-doped fiber amplifier (EDFA) to 23 dBm, and then injected into the FUT. The reflected light (Stokes) was amplified using another EDFA to 3 dBm and mixed using another optical coupler with the reference light, which passed through a ~1 km long delay line. The heterodyned Brillouin signal, which was converted into an electrical signal with a photo detector (PD), was mixed with the output

Fig. 1 Basic configuration of high-speed BOCADR. **a** Experimental setup. AMP amplifier; BPF band-pass filter; DAQ data acquisition; EDFA erbium-doped fiber amplifier; ESA electrical spectrum analyzer; FG function generator; FUT fiber under test; IF intermediate frequency; LO local oscillator; LPF low-pass filter; MFS microwave frequency sweeper; MG microwave generator; NFL noise floor; OSC oscilloscope; PD photo detector; PSCR polarization scrambler; RF radio frequency. **b** Normalized direct output from the ESA (green), noise floor (blue), and the intrinsic BGS obtained as their difference (red). **c** Measured BFS dependence on a relatively large strain of up to 2.0%. The orange solid circles are measured points, whereas the blue line is a linear fit. Copyright (2017) The Japan Society of Applied Physics (JSAP)



of a microwave frequency sweeper (MFS), the frequency of which can be repeatedly swept over a range of several hundred megahertz. The power at a fixed frequency component (carefully selected) of the mixed signal was then output from the ESA, which repeatedly provided the BGS in the time domain (see Fig. 2). Next, it was input to the computer via an inexpensive sound board (XONAR U7; ASUSTek) and monitored using a virtual oscilloscope triggered at the repetition frequency of the MFS. The BGS was observed on a real-time basis, but was largely distorted because of the considerable intensity noise of the MFS output, which was dependent on the applied voltage (or output frequency). To suppress this noise and clearly observe the BGS, the differential signal between periods of operation with and without the Brillouin signal (i.e. between the two spectra for which the 980 nm pump LD of the EDFA in the Brillouin-pump path is and is not working) was calculated. It was finally acquired as the BGS after low-pass filtering.

2.2 Fundamental characterization

Here, an MFS with a maximal repetition rate of 50 Hz was used. First, we verified that the local BGS can be correctly observed at this frequency. A 7.0 m long silica SMF (composed of a 0.8 m long pigtail of an optical circulator connected to a 6.2 m long SMF using an FC/APC adaptor) was used as the FUT. The open end was cut at an angle of 8° to suppress the Fresnel reflection. The modulation frequency f_m was set to 13.536 MHz, with a correlation peak located at the point 4.7 m away from the circulator. The measurement range d_m was calculated to be 7.6 m according to Eq. (1). The modulation amplitude Δf was set to 0.5 GHz, resulting in a theoretical spatial resolution Δz of ~ 0.15 m from Eq. (2). The ratio of the measurement range to the spatial

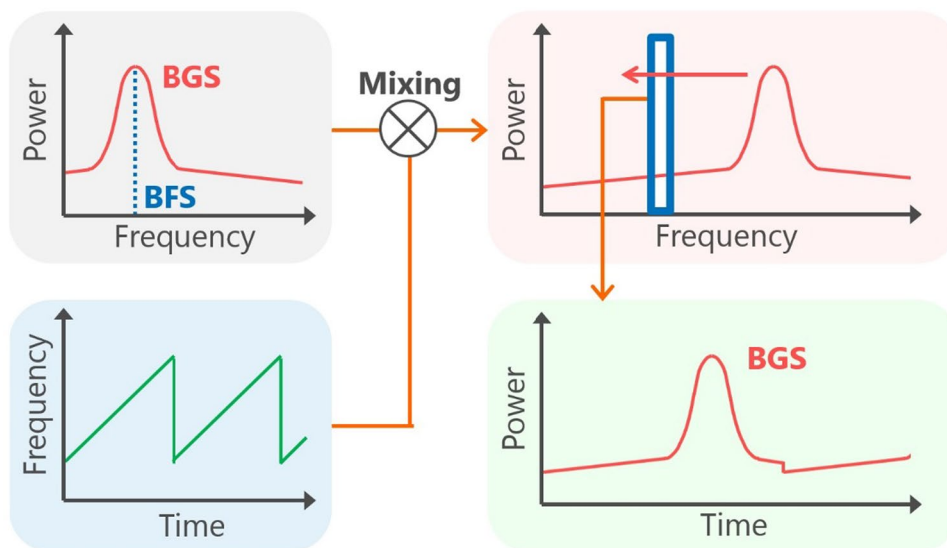
resolution was 51, which can be extended to ~ 570 simply by increasing Δf to half of the BFS, i.e. ~ 5.4 GHz (The Δf values were kept below 1.5 GHz in this paper to avoid damage to the laser, which was not designed for high-frequency modulation use). The 64th correlation peak was used; the temperature of the room was 18°C .

The green curve in Fig. 1b shows the direct output from the ESA (the vertical axis was normalized in a linear scale so that the maximal voltage of this spectrum became 1), which suffers from considerable noise, making it difficult to determine the BFS. To suppress this noise, the noise floor, i.e. the spectrum when the EDFA in the pump path was switched off, was recorded (blue curve in Fig. 1b) and subtracted from the ESA output, resulting in the intrinsic BGS as shown the red curve in Fig. 1b. The dip at ~ 11.3 GHz, which originates from the sharp spectral noise due to the frequency range switching of the MFS, can be flattened with an appropriate low-pass filter (LPF). Thus, it was confirmed that the local BGS was obtained at 50 Hz. Note that a higher sampling rate can be achieved simply using a higher-speed frequency sweeper (also refer to Sect. 3.1).

2.3 Demonstration of wide strain dynamic range

We then demonstrated a measurement with a wide strain dynamic range. The experimental conditions were the same as those for evaluating the noise floor described above. In the 7.0 m long SMF used as the FUT, strains of up to 2.0% were applied to a 0.4 m long section (4.5–4.9 m away from the circulator) fixed on a translation stage (Fig. 3a). The correlation peak was located at the midpoint of the strained section. The average of 5 measurements revealed the sampling rate of 10 Hz. Figure 4 shows the measured BGS dependence on strain. Note that all the BGSs were normalized. With

Fig. 2 Principle of high-speed BGS acquisition. By mixing with a frequency-swept microwave, the BGS originally observed in the frequency domain can be obtained in the time domain at high speed. Copyright (2016) Nature Publishing Group (NPG)



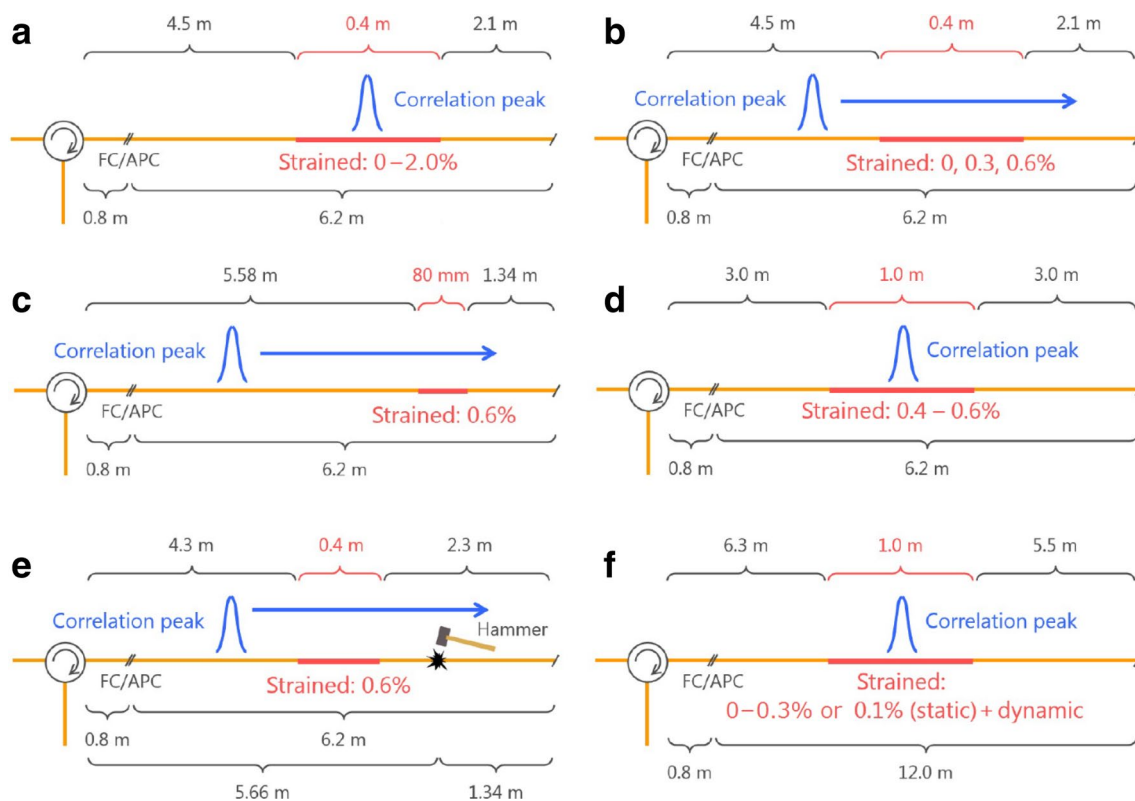


Fig. 3 Structures of FUTs. **a** Fixed-point measurement of static strain. **b** Distributed measurement with a higher SNR. **c** Distributed measurement with a higher spatial resolution. **d** Fixed-point measurement

of dynamic strain (not sinusoidally applied; see Fig. 6). **e** Distributed measurement for breakage detection. **f** Fixed-point measurement of dynamic strain (sinusoidally applied). Copyright (2017) JSAP

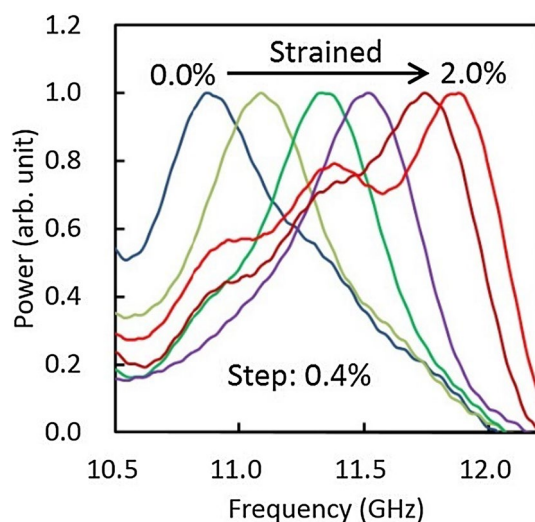


Fig. 4 Measured BGS dependence on a relatively large strain. Copyright (2017) JSAP

increasing strain, the BGS shifted to a higher frequency. At 2.0% strain, the translation stages began to slightly slip, at which point the correct amount of strain could not be applied; besides, at such large strain, considerable optical loss was

engendered at the fixed (and pressed) positions, resulting in a weak BGS, which was distorted if normalized. Figure 1c shows the BFS dependence on strain, which was almost linear. The slope calculated using the data (excluding that of the 2.0% strain) was 509.5 MHz/%, which moderately agrees with the previously reported values at 1550 nm [31, 41]. Thus, the wide strain dynamic range of ~2.0% was demonstrated. The maximal measurable strain, which is about three times the largest value previously reported for BOCDR [36], is even close to the fracture strain of silica SMFs, which is generally several percent.

2.4 Distributed and dynamic strain measurements

Distributed measurements were subsequently demonstrated. First, a 7.0 m long silica SMF was used as the FUT, in which strains of 0.3 and 0.6% were applied to a 0.4 m long section (4.5–4.9 m) (Fig. 3b). The modulation frequency f_m was swept from 13.406 to 13.601 MHz. The measurement range d_m was calculated to be ~7.6 m. The modulation amplitude Δf was set to 0.5 GHz, corresponding to the nominal spatial resolution Δz of ~0.15 m. The sampling rate for obtaining one BGS was 50 Hz and the number of sensing points was 200, resulting in a measurement time of ~4 s. The measured

BGS distributions (normalized) are shown in Fig. 5a–c, and the corresponding BFS distributions are shown in Fig. 5d, where the strained sections were correctly detected with a high SNR. The non-normalized data are discussed in Sect. 2.5.

Next, a 0.6% strain was applied to an 80 mm long section (5.58–5.66 m) of the same FUT (Fig. 3c), and Δf was set to 1.5 GHz, corresponding to Δz of ~ 48 mm. The measured BGS distribution is shown in Fig. 5e, and the magnified view of the BFS distribution around the strained section is shown in Fig. 5f. Although the SNR deteriorated because of the enhanced spatial resolution, the strained section was successfully detected.

We also demonstrated the capability of dynamic strain sensing. A 0.4% static strain was applied in advance to a 1.0 m long section (3.0–4.0 m) of a 7.0 m long silica SMF (Fig. 3d); the static strain was applied because it was difficult to stably apply dynamic strains to an unstrained section. Dynamic strains at 2.2 and 4.0 Hz were then applied to the strained section, not sinusoidally, using a rotor with a 33 mm long arm (Fig. 6). By setting f_m to 13.503 GHz, the correlation peak was placed at the midpoint of the strained section ($d_m = \sim 7.6$ m). The spatial resolution Δz was ~ 0.36 m

($\Delta f = 0.2$ GHz), and the sampling rate was 50 Hz. No averaging was performed. The measured temporal variations of the BGS and BFS at 2.2 Hz (Fig. 7a, b) and at 4.0 Hz (Fig. 7c, d) indicate that the dynamic strains were successfully detected with a much higher SNR than in a previous report [33].

2.5 Breakage detection

We finally demonstrated the detection of a breakage point caused during a distributed measurement. A 7.0 m long silica SMF was used as the FUT, in which a 0.6% strain was applied to a 0.4 m long section (4.3–4.7 m). The measurement range d_m was ~ 7.6 m (f_m swept from 13.406 to 13.601 MHz) and the nominal spatial resolution Δz was ~ 0.15 m ($\Delta f = 0.5$ GHz). Then, during a distributed measurement, the FUT was broken by being crushed with a hammer at a location 5.66 m away from the circulator (Fig. 3e). The normalized BGS distributions along the FUT measured before and after the FUT was broken (Fig. 8a, b) clearly indicate that, when the FUT is broken at a point, the measurement can still continue to the breakage point. However, in the section beyond the breakage point, the normalized spectra were significantly distorted.

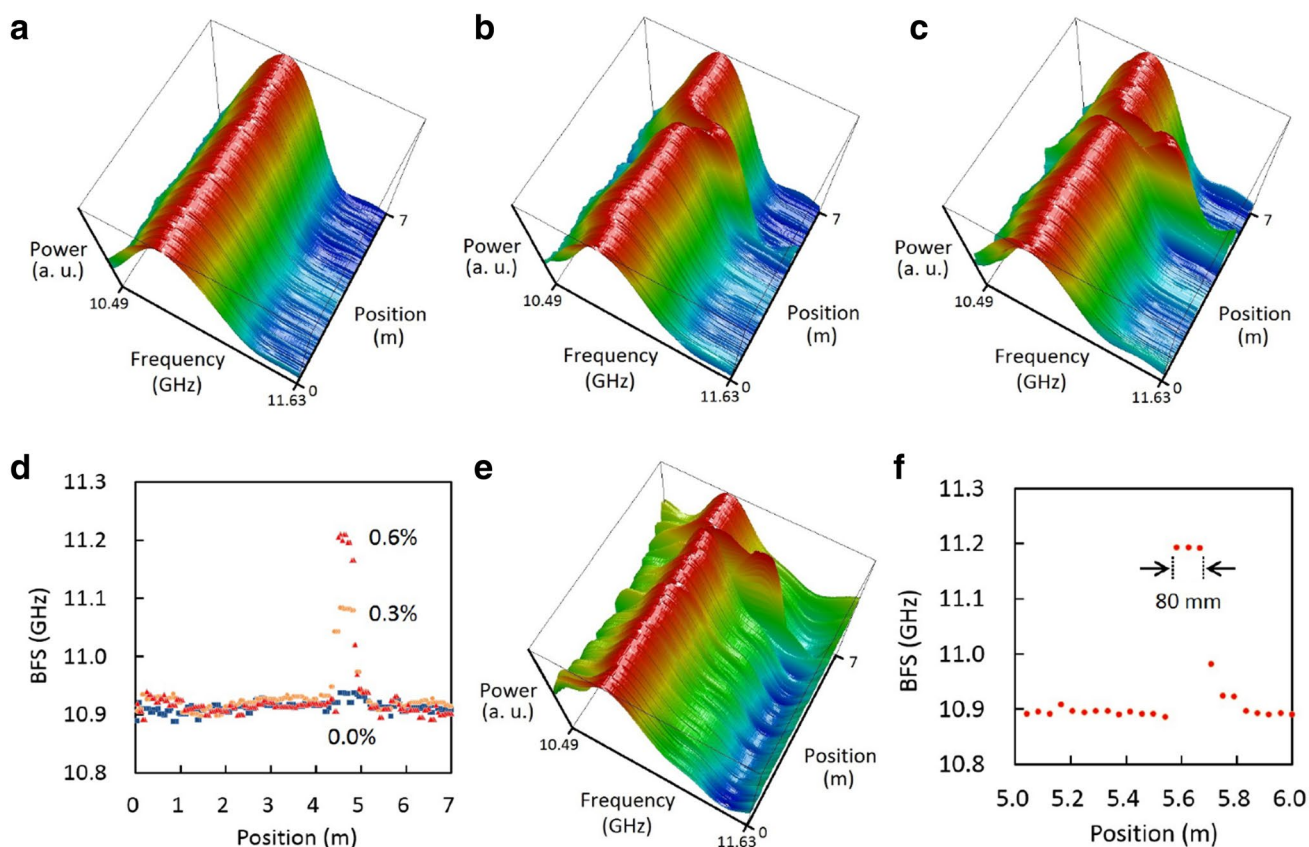


Fig. 5 Distributed measurement results. **a–c** BGS distributions for locally applied strains of 0.0, 0.3, and 0.6%, respectively. **d** Corresponding BFS distributions. **e** BGS distribution for a locally applied 0.6% strain. **f** Corresponding BFS distribution (magnified). Copyright (2017) JSAP

Fig. 6 Method for applying dynamic strain (0.4–0.6%) to a fixed section of the FUT using an armed rotor. Copyright (2017) JSAP

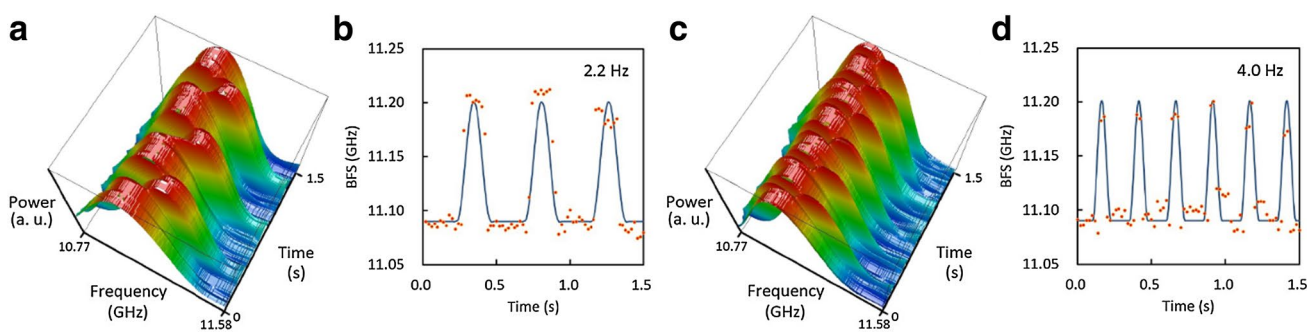
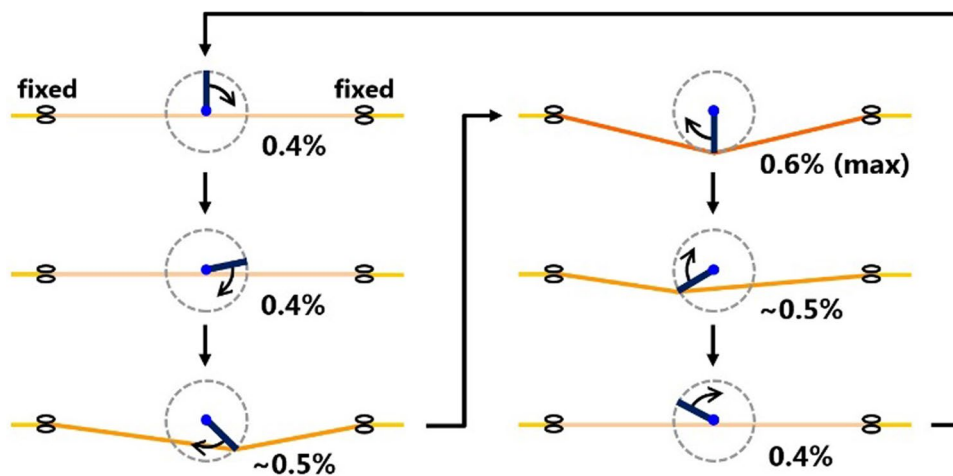


Fig. 7 Measurement results of dynamic strain. Temporal variation of **a** BGS and **b** BFS at 2.2 Hz, as well as **c** BGS and **d** BFS at 4.0 Hz. The circles are measured points, whereas the solid curves indicate the theoretical trends. Copyright (2017) JSAP

Fig. 8 Normalized BGS distributions. Data measured **a** before and **b** after the FUT was broken at 5.66 m. Copyright (2017) JSAP

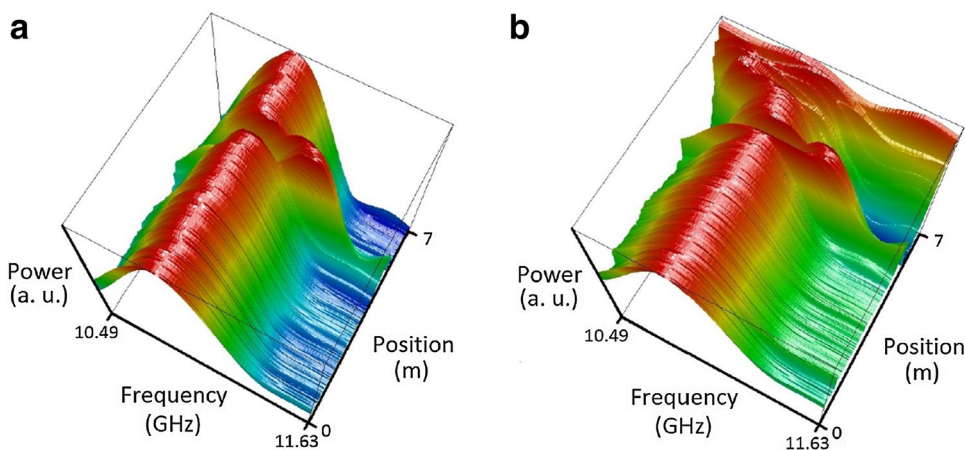


Figure 9a, b show the non-normalized data corresponding to Fig. 8a, b, respectively. From these figures, the peak-power distributions were derived (Fig. 9c). Before the FUT was broken, a slight spectral jump was observed at 0.8 m, which corresponds to the location at which the FC/APC adaptor connects the pigtail of the circulator and the silica SMF. A spectral dip was also observed at ~4.5 m, corresponding to the applied strain. The peak power of the

BGS at the strained section becomes lower than that at the unstrained section, because the weak but non-zero Brillouin signals of the correlation peak sidelobes (generally located at the unstrained sections) do not overlap. After the FUT was broken at 5.66 m, and while the spectral jump at 0.8 m and the dip at ~4.5 m were maintained, the peak power at the section beyond the breakage point decreased drastically. This is reasonable considering that almost no Brillouin signal

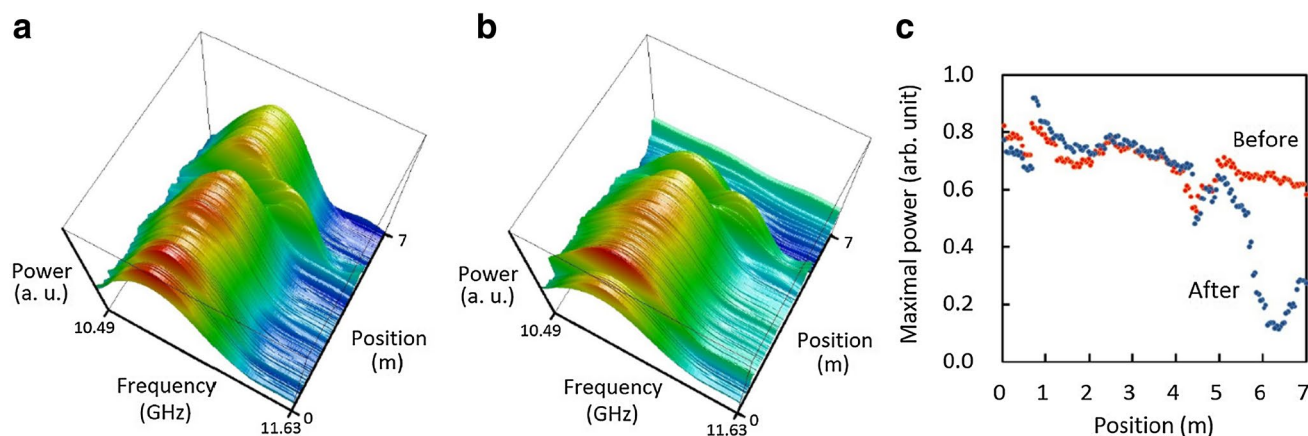


Fig. 9 Results of breakage detection. Non-normalized BGS distributions measured **a** before and **b** after the FUT was broken at 5.66 m. **c** Peak-power distribution measured before the FUT was broken (red), and after the FUT was broken (blue). Copyright (2017) JSAP

returns from where the correlation peak is located, which also explains the distorted normalized spectra (Fig. 8b). Therefore, if a certain threshold power is appropriately set (for instance, 0.4 in Fig. 9c), we can perform real-time detection of the breakage location.

3 Ultrahigh-speed configuration: phase-detected BOCDR

3.1 Proposal

It is crucial to distributed measurements of dynamic strain at higher frequencies (up to the order of kilohertz) to further enhance the operating speed of the BOCDR system. One simple solution is to replace the MFS with a VCO, the frequency of which can be swept across a range of several hundred megahertz at a much higher repetition rate. As the output frequency of the VCO is not necessarily linearly dependent on the input voltage, a so-called pre-distortion technique should be employed. However, the enhancement of the sampling rate of the BFS is limited to several hundreds of hertz by the mere use of the VCO, because the BGS acquisition (determined by the repetition rate of the VCO) must be slower than the calculation time required for the BFS derivation from the BGS.

To tackle this issue, we developed a method for simultaneously deriving the BFS and the BGS [39]. The experimental configuration is depicted in Fig. 10a, where the MFS in Fig. 1a is replaced by a VCO that is driven with a sinusoidal output from a function generator. The basic concept of the subsequent signal processing is shown in Fig. 11. The ESA output, which can be regarded as the BGS, was approximated by a one-period sinusoidal waveform using a band-pass filter (BPF) with the same central frequency as

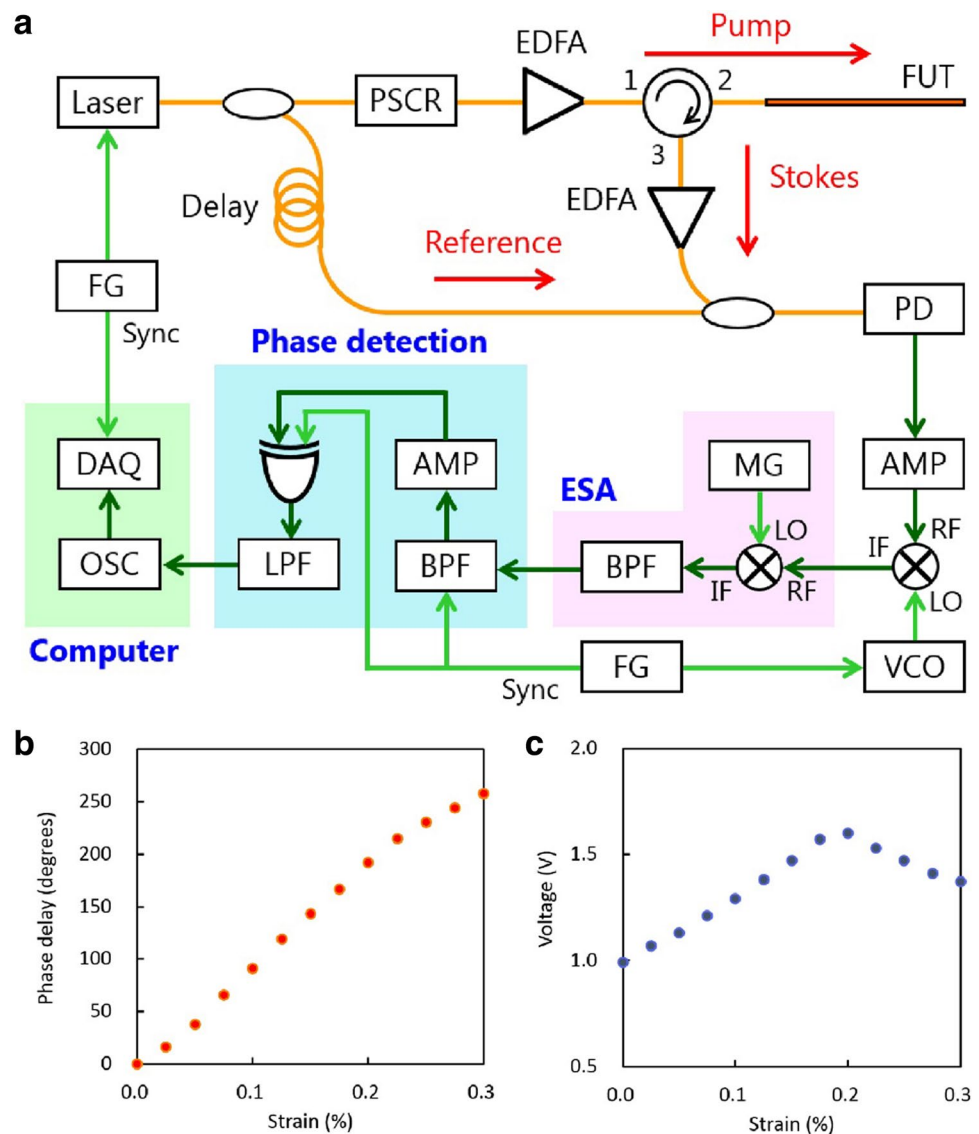
the repetition rate of the VCO. At this stage, the BFS was in one-to-one correspondence with the phase delay of the sinusoidal waveform (at the expense of the limited range of measurable strain), which was detected using an electrical amplifier, an exclusive-OR (XOR) logic gate, and an LPF. With this configuration, only a phase delay smaller than 180° can be properly detected. The phase delay was finally monitored as a quasi-DC voltage using a virtual oscilloscope implemented in a personal computer, triggered by the repetition frequency for the distributed measurement. Note that all of the additionally employed devices are relatively inexpensive. This ultrahigh-speed configuration is named phase-detected BOCDR.

3.2 Operation confirmation

First, the VCO operation with a BFS sampling rate of 100 kHz was confirmed (An even higher sampling rate was achievable if the SNR deterioration was admitted). When the frequency-control voltage was linearly applied to the VCO (blue line in Fig. 12a), the output frequency was distorted (blue curve in Fig. 12b) because of the nonlinear frequency dependence on the applied voltage. Therefore, we applied a pre-distorted voltage (red curve in Fig. 12a) and obtained the linear output frequency (red line in Fig. 12b).

We then verified that the phase delay and the final DC voltage were in one-to-one correspondence with the applied strain. In the 12.8 m long SMF used as the FUT, strains of up to 0.3% were applied to a 1.0 m long section (6.3–7.3 m) (Fig. 3f). The correlation peak was located at the midpoint of the strained section by setting f_m to 7.222 MHz ($d_m = \sim 14.2$ m), and the spatial resolution Δz was ~ 0.38 m ($\Delta f = 0.35$ GHz). The strain dependence of the normalized BGS approximated by a one-period sinusoidal waveform (Fig. 13) shows that the phase is delayed with increasing

Fig. 10 Configuration of ultrahigh-speed BOCDR. **a** Experimental setup. *AMP* amplifier; *BPF* band-pass filter; *DAQ* data acquisition; *EDFA* erbium-doped fiber amplifier; *ESA* electrical spectrum analyzer; *FG* function generator; *FUT* fiber under test; *IF* intermediate frequency; *LO* local oscillator; *LPF* low-pass filter; *MG* microwave generator; *OSC* oscilloscope; *PD* photo detector; *PSCR* polarization scrambler; *RF* radio frequency; *VCO* voltage-controlled oscillator. **b** Measured phase delay and **c** output DC voltage plotted as functions of applied strain. Copyright (2016) NPG



strain. The strain dependence of the phase delay (Fig. 10b) was almost linear up to 0.2% with a slope of $943^\circ/\%$ (calculated excluding the data at $>0.2\%$, which deviated from the linear trend). The DC voltage, i.e. the output from the LPF (cut-off frequency = 1.2 kHz) was also plotted as a function of applied strain (Fig. 10c). The voltage increases linearly with increasing strain (slope = $3.2 \text{ V}/\%$) and reaches a maximum at $\sim 0.2\%$, where the phase delay becomes 180° . At this stage, it decreases for strains beyond 0.2%. Thus, the DC voltage was verified to correspond to the applied strain.

3.3 Dynamic strain measurement

A static strain of 0.1% was applied to a 1.0 m long section of the 12.8 m long FUT (6.3–7.3 m) (Fig. 3f). Dynamic strains at 30, 100, 300 Hz, and 1 kHz were then additionally applied to the same section using a vibration generator. Averaging

was performed 10 times on the virtual oscilloscope. The other experimental conditions were the same as those for the operation confirmation described above. The measured temporal variations of the output voltage (Fig. 14a–d) indicate that the dynamic strains of up to 1 kHz were successfully detected, though the data at 1 kHz were somewhat distorted. The vibration amplitude, which is dependent on the vibration frequency, can be derived from Fig. 10c; for instance, at 30 Hz, the applied strain ranges from 0.02 to 0.18%, corresponding to a vibration amplitude of 0.8 mm. This value moderately agreed with the directly measured value using a laser Doppler velocimeter.

3.4 Tracking of mechanical wave propagation

Finally, to demonstrate the system's capability for ultrahigh-speed acquisition of the strain distribution, we attempted

Fig. 11 Principle of high-speed BFS acquisition. The BGS is approximated by a one-period sinusoidal waveform and rectified. Its phase delay, which corresponds to the BFS, is then detected using an XOR logic gate and a LPF. The output voltage is in one-to-one correspondence with the phase delay in the range from 0 to 180°. Copyright (2016) NPG

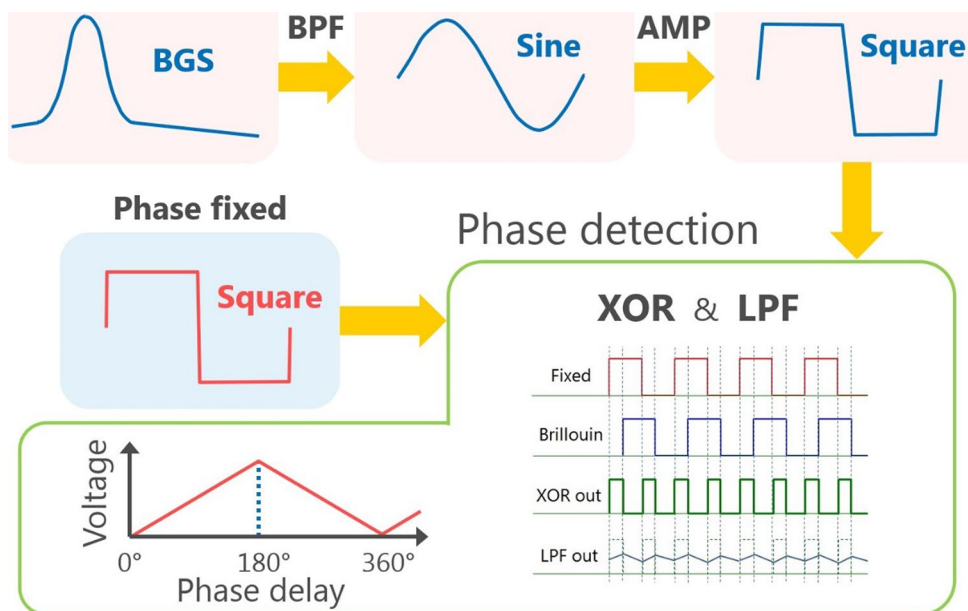
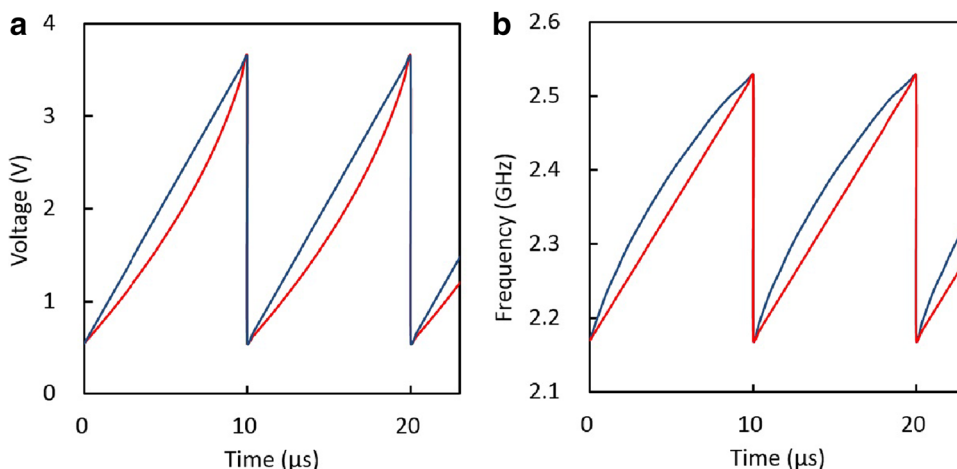


Fig. 12 VCO operation with a BFS sampling rate of 100 kHz. **a** Linearly applied voltage (blue) and pre-distorted applied voltage (red). **b** Output frequencies when the voltage was applied in linear (blue) and pre-distorted (red) manners. Copyright (2016) NPG



to track the propagation of a mechanical wave [42] along the FUT. The structure of the FUT is depicted in Fig. 14e, where a 3.2 m long section (6.0–9.2 m) was tightly adhered to a 0.1 m wide, 1 mm thick rubber sheet using tape. Note that the newly employed 4.8 m long SMF (0.8–5.6 m) had a slightly lower BFS (~ 10.8 GHz) than that of the 12.0 m long SMF (5.6–17.6 m). A mechanical wave was manually generated (Fig. 14f) and propagated along the rubber-adhered section at a relatively slow speed. The sampling rate of the BFS (or strain) was set to 100 kHz, and the repetition rate of the distributed measurement was set to 100 Hz. Averaging was performed 10 times. The measurement range d_m was ~ 20.4 m (f_m swept from 5.048 to 5.153 MHz; 24th correlation peak) and the nominal spatial resolution Δz was ~ 0.39 m ($\Delta f = 0.5$ GHz).

The measured temporal variation of the strain distribution around the 3.2 m long section attached to the rubber

sheet (Fig. 14g) shows that the mechanical wave propagation was detected, though the SNR was low. The propagation speed was calculated to be approximately 10 m/s. The length of the strained section and the amplitude of the strain decreased as the mechanical wave propagated. The amount of strain caused by the wave propagation ($< 0.03\%$) seems to be valid, as it is close to that measured by two-end-access BOTDA [42]. The amount of strain along the 4.8 m long SMF with a lower BFS was not correctly detected (negative values obtained), which is reasonable considering the operating principle that limits the measurable strain range. Thus, the ultrahigh-speed distributed strain sensing capability of this system was demonstrated.

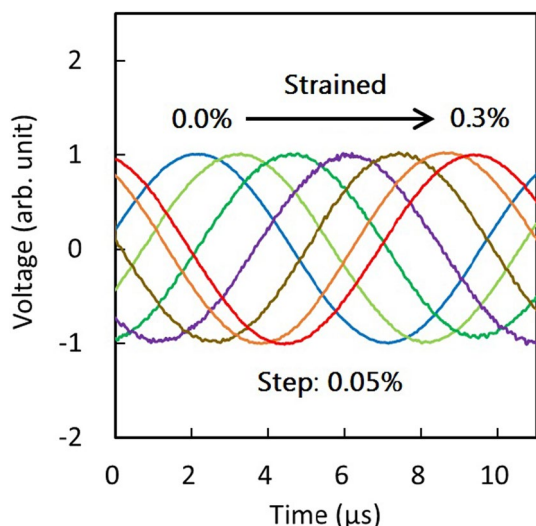


Fig. 13 Strain dependence of the normalized BGS approximated by a one-period sinusoidal waveform. Copyright (2016) NPG

4 Conclusions

We reviewed the recent development of high-speed configurations of BOCDR, including phase-detected BOCDR, which can perform real-time distributed measurement with intrinsic one-end accessibility, high spatial resolution, and wide strain dynamic range. Compared to conventional two-end-access systems, BOCDR offers a high degree of freedom in embedding the sensors into materials and structures, and can continuously perform measurements even when extremely high loss or breakage occurs at a point along the sensing fiber. Another advantage to be emphasized here is the cost efficiency of the system. Besides the fact that the experimental setup does not involve EOMs, which are used in most conventional Brillouin sensors, all of the newly employed electrical devices, which include a VCO, filter, mixer, sound board, etc., are relatively inexpensive. Further cost reduction can be achieved by replacing the ESA with a specialized circuit, which also contributes to downsizing the whole system. In the meantime,

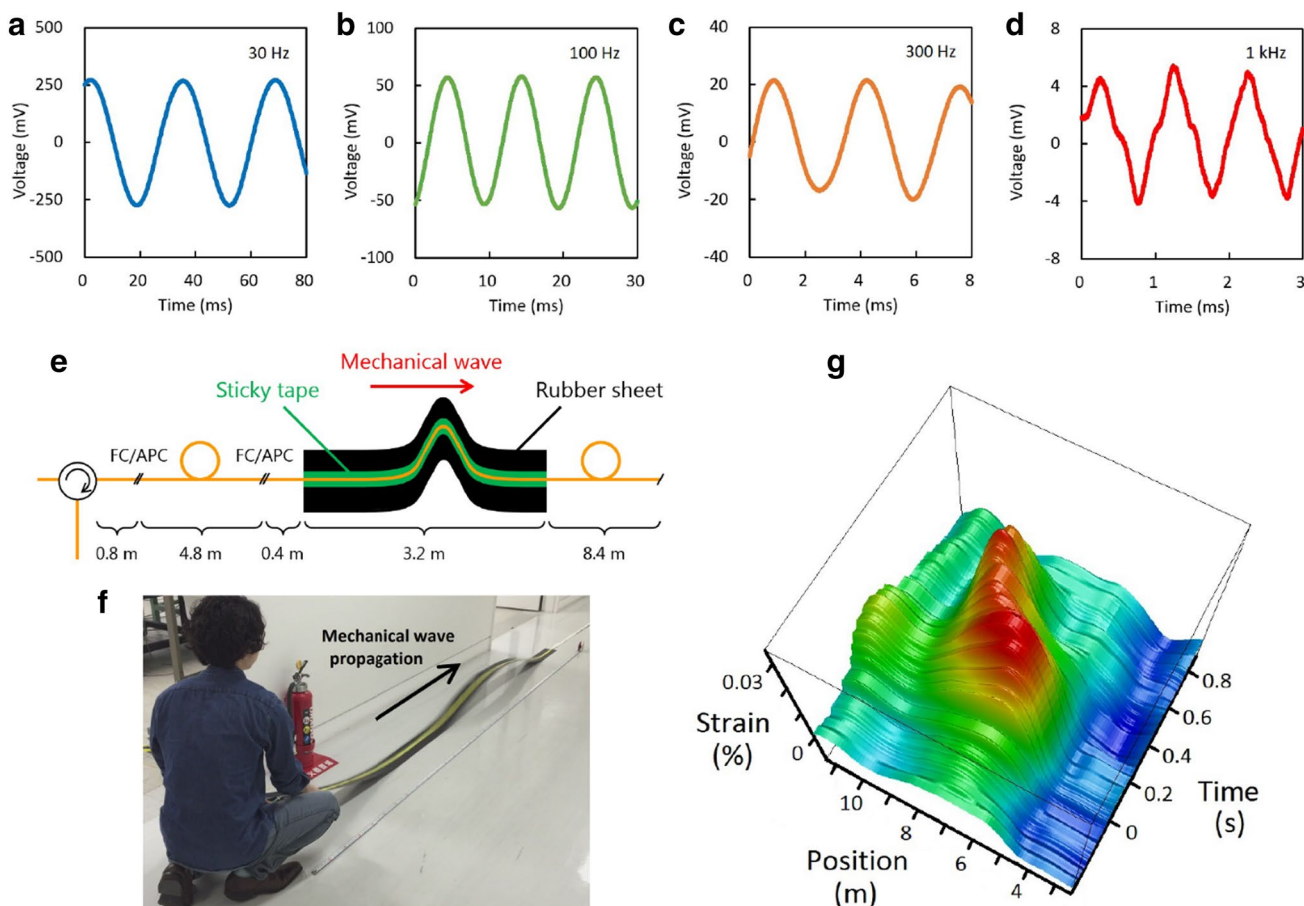


Fig. 14 Ultrahigh-speed measurement results. Temporal variations of the output voltage when dynamic strains were applied to a 1.0 m long section at **a** 30 Hz, **b** 100 Hz, **c** 300 Hz, and **d** 1 kHz. **e** Schematic

structure and **f** photograph of the FUT while tracking the propagation of a mechanical wave. **g** Measured temporal variation of the strain distribution. Copyright (2016) NPG

this system suffers from a trade-off between the spatial resolution and the measurement range. Their ratio is limited to ~ 570 in a basic configuration, though some techniques for improving this value have been developed [12, 34]. We thus anticipate that phase-detected BOCDR will be a promising technique for distributed dynamic strain and temperature sensing with high spatial resolution, especially for a relatively short measurement range. We have also been developing another real-time configuration of BOCDR, called slope-assisted BOCDR [43–46], the detailed description of which is out of the scope of this paper.

Acknowledgements The authors wish to acknowledge Tomohito Kawa, Heeyoung Lee, Shumpei Shimada, Makoto Shizuka, Kazunari Minakawa, Hiroki Tanaka, Sho Ikeda, Daisuke Yamane, Hiroyuki Ito, Shiro Doshō, and Kazuya Masu (Institute of Innovative Research, Tokyo Institute of Technology) for their experimental assistance. This work was supported by JSPS KAKENHI Grant Numbers 25709032, 26630180, 25007652, and 17H04930, and by research Grants from the Iwatani Naoji Foundation, the SCAT Foundation, the Konica Minolta Science and Technology Foundation, the Japan Gas Association, the ESPEC Foundation for Global Environment Research and Technology, the Association for Disaster Prevention Research, the Fujikura Foundation, and the Japan Association for Chemical Innovation.

Compliance with ethical standards

Conflict of interest On behalf of all authors, the corresponding author states that there is no conflict of interest.

References

1. Agrawal, G.P.: *Nonlinear Fiber Optics*. Academic, Cambridge (2001)
2. Horiguchi, T., Tateda, M.: BOTDA—nondestructive measurement of single-mode optical fiber attenuation characteristics using Brillouin interaction: theory. *J. Lightwave Technol.* **7**, 1170–1176 (1989)
3. Voskoboinik, A., et al.: SBS-based fiber optical sensing using frequency-domain simultaneous tone interrogation. *J. Lightwave Technol.* **29**, 1729–1735 (2011)
4. Bernini, R., Minardo, A., Zeni, L.: Dynamic strain measurement in optical fibers by stimulated Brillouin scattering. *Opt. Lett.* **34**, 2613–2615 (2009)
5. Peled, Y., Motil, A., Yaron, L., Tur, M.: Slope-assisted fast distributed sensing in optical fibers with arbitrary Brillouin profile. *Opt. Express* **19**, 19845–19854 (2011)
6. Peled, Y., Motil, A., Tur, M.: Fast Brillouin optical time domain analysis for dynamic sensing. *Opt. Express* **20**, 8584–8591 (2012)
7. Taki, M., et al.: Cyclic pulse coding for fast BOTDA fiber sensors. *Opt. Lett.* **38**, 2877–2880 (2013)
8. Danon, O., Motil, A., Sovran, I., Hadar, R., Tur, M.: Real-time fast and distributed measurement of a Brillouin-inhomogeneous fiber using tailored-frequency probe in slope-assisted BOTDA. *Proc. SPIE* **9157**, 9157AM (2014)
9. Muanenda, Y., Taki, M., Pasquale, F.D.: Long-range accelerated BOTDA sensor using adaptive linear prediction and cyclic coding. *Opt. Lett.* **39**, 5411–5414 (2014)
10. Sovran, I., Motil, A., Tur, M.: Frequency-scanning BOTDA with ultimately fast acquisition speed. *IEEE Photon. Technol. Lett.* **27**, 1426–1429 (2015)
11. Dong, Y., et al.: High-spatial-resolution fast BOTDA for dynamic strain measurement based on differential double-pulse and second-order sideband of modulation. *IEEE Photon. J.* **5**, 2600407 (2013)
12. Elooz, D., Antman, Y., Levanon, N., Zadok, A.: High-resolution long-reach distributed Brillouin sensing based on combined time-domain and correlation-domain analysis. *Opt. Express* **22**, 6453–6463 (2014)
13. Garus, D., Krebber, K., Schliep, F., Gogolla, T.: Distributed sensing technique based on Brillouin optical-fiber frequency-domain analysis. *Opt. Lett.* **21**, 1402–1404 (1996)
14. Bernini, R., Minardo, A., Zeni, L.: Distributed sensing at centimeter-scale spatial resolution by BOFDA: measurements and signal processing. *IEEE Photon. J.* **4**, 48–56 (2012)
15. Minardo, A., Bernini, R., Zeni, L.: Distributed temperature sensing in polymer optical fiber by BOFDA. *IEEE Photon. Technol. Lett.* **26**, 387–390 (2014)
16. Wosniok, A., Mizuno, Y., Krebber, K., Nakamura, K.: L-BOFDA: a new sensor technique for distributed Brillouin sensing. *Proc. SPIE* **8794**, 879431 (2013)
17. Hotate, K., Hasegawa, T.: Measurement of Brillouin gain spectrum distribution along an optical fiber using a correlation-based technique—proposal, experiment and simulation. *IEICE Trans. Electron.* **E83-C**, 405–412 (2000)
18. Song, K.Y., He, Z., Hotate, K.: Distributed strain measurement with millimeter-order spatial resolution based on Brillouin optical correlation domain analysis. *Opt. Lett.* **31**, 2526–2528 (2006)
19. Song, K.Y., Hotate, K.: Distributed fiber strain sensor at 1 kHz sampling rate based on Brillouin optical correlation domain analysis. *IEEE Photon. Technol. Lett.* **19**, 1928–1930 (2007)
20. Song, K.Y., Kishi, M., He, Z., Hotate, K.: High-repetition-rate distributed Brillouin sensor based on optical correlation-domain analysis with differential frequency modulation. *Opt. Lett.* **36**, 2062–2064 (2011)
21. Song, K.Y., Hotate, K.: Brillouin optical correlation domain analysis in linear configuration. *IEEE Photon. Technol. Lett.* **20**, 2150–2152 (2008)
22. Jeong, J.H., et al.: Linearly configured BOFDA system using a differential measurement scheme. *Opt. Express* **22**, 1467–1473 (2014)
23. Song, K.Y., He, Z., Hotate, K.: Optimization of Brillouin optical correlation domain analysis system based on intensity modulation scheme. *Opt. Express* **14**, 4256–4263 (2006)
24. Zhang, C., Kishi, M., Hotate, K.: 5,000 points/s high-speed random accessibility for dynamic strain measurement at arbitrary multiple points along a fiber by Brillouin optical correlation domain analysis. *Appl. Phys. Express* **8**, 042501 (2015)
25. Kurashima, T., Horiguchi, T., Izumita, H., Furukawa, S., Koyamada, Y.: Brillouin optical-fiber time domain reflectometry. *IEICE Trans. Commun.* **E76-B**, 382–390 (1993)
26. Alahbabi, M.N., Cho, Y.T., Newson, T.P.: 100 km distributed temperature sensor based on coherent detection of spontaneous Brillouin backscatter. *Meas. Sci. Technol.* **15**, 1544–1547 (2004)
27. Geng, J., Staines, S., Blake, M., Jiang, S.: Distributed fiber temperature and strain sensor using coherent radio-frequency detection of spontaneous Brillouin scattering. *Appl. Opt.* **46**, 5928–5932 (2007)
28. Masoudi, A., Belal, M., Newson, T.P.: Distributed dynamic large strain optical fiber sensor based on the detection of spontaneous Brillouin scattering. *Opt. Lett.* **38**, 3312–3315 (2013)
29. Tu, G., Zhang, X., Zhang, Y., Ying, Z., Lu, L.: Strain variation measurement with short-time Fourier transform-based Brillouin

- optical time-domain reflectometry sensing system. *Electron. Lett.* **50**, 1624–1626 (2014)
30. Minardo, A., Bernini, R., Ruiz-Lombera, R., Mirapeix, J., Lopez-Higuera, L.M., Zeni, L.: Proposal of Brillouin optical frequency-domain reflectometry (BOFDR). *Opt. Express* **24**, 29994–30001 (2016)
 31. Mizuno, Y., Zou, W., He, Z., Hotate, K.: Proposal of Brillouin optical correlation-domain reflectometry (BOCDR). *Opt. Express* **16**, 12148–12153 (2008)
 32. Mizuno, Y., Zou, W., He, Z., Hotate, K.: Operation of Brillouin optical correlation-domain reflectometry: theoretical analysis and experimental validation. *J. Lightwave Technol.* **28**, 3300–3306 (2010)
 33. Mizuno, Y., He, Z., Hotate, K.: One-end-access high-speed distributed strain measurement with 13-mm spatial resolution based on Brillouin optical correlation-domain reflectometry. *IEEE Photon. Technol. Lett.* **21**, 474–476 (2009)
 34. Mizuno, Y., He, Z., Hotate, K.: Measurement range enlargement in Brillouin optical correlation-domain reflectometry based on temporal gating scheme. *Opt. Express* **17**, 9040–9046 (2009)
 35. Mizuno, Y., He, Z., Hotate, K.: Stable entire-length measurement of fiber strain distribution by Brillouin optical correlation-domain reflectometry with polarization scrambling and noise-floor compensation. *Appl. Phys. Express* **2**, 062403 (2009)
 36. Manotham, S., Kishi, M., He, Z., Hotate, K.: 1-cm spatial resolution with large dynamic range in strain distributed sensing by Brillouin optical correlation domain reflectometry based on intensity modulation. *Proc. SPIE* **8351**, 835136 (2012)
 37. Koizumi, K., Kanda, Y., Fujii, A., Murai, H.: High-speed distributed strain measurement using Brillouin optical time-domain reflectometry based-on self-delayed heterodyne detection. *Proc. ECOC* (2015). <https://doi.org/10.1109/ECOC.2015.7341700>
 38. Mizuno, Y., Hayashi, N., Fukuda, H., Nakamura, K.: Single-end-access distributed strain sensing with wide dynamic range using higher-speed Brillouin optical correlation-domain reflectometry. *Jpn. J. Appl. Phys.* **56**, 072501 (2017)
 39. Mizuno, Y., Hayashi, N., Fukuda, H., Song, K.Y., Nakamura, K.: Ultrahigh-speed distributed Brillouin reflectometry. *Light: Sci. Appl.* **5**, e16184 (2016)
 40. Hotate, K., He, Z.: Synthesis of optical-coherence function and its applications in distributed and multiplexed optical sensing. *J. Lightwave Technol.* **24**, 2541–2557 (2006)
 41. Horiguchi, T., Kurashima, T., Tateda, M.: Tensile strain dependence of Brillouin frequency shift in silica optical fibers. *IEEE Photon. Technol. Lett.* **1**, 107–108 (1989)
 42. Peled, Y., Motil, A., Kressel, I., Tur, M.: Monitoring the propagation of mechanical waves using an optical fiber distributed and dynamic strain sensor based on BOTDA. *Opt. Express* **21**, 10697–10705 (2013)
 43. Lee, H., Hayashi, N., Mizuno, Y., Nakamura, K.: Slope-assisted Brillouin optical correlation-domain reflectometry: proof of concept. *IEEE Photon. J.* **8**, 6802807 (2016)
 44. Lee, H., Hayashi, N., Mizuno, Y., Nakamura, K.: Operation of slope-assisted Brillouin optical correlation-domain reflectometry: comparison of system output with actual frequency shift distribution. *Opt. Express* **24**, 29190–29197 (2016)
 45. Lee, H., Hayashi, N., Mizuno, Y., Nakamura, K.: Slope-assisted Brillouin optical correlation-domain reflectometry using polymer optical fibers with high propagation loss. *J. Lightwave Technol.* **35**, 2306–2310 (2017)
 46. Lee, H., Mizuno, Y., Nakamura, K.: Measurement sensitivity dependencies on incident power and spatial resolution in slope-assisted Brillouin optical correlation-domain reflectometry. *Sensors Actuators A Phys.* **268**, 68–71 (2017)